Image Dehazing Based on Sigmoid-guided filtering-Retinex in NSCT Domain

Yuanbin Wang, Bingchao Wu, and Zongyou Duan

***Abstract*—Foggy images suffer from severe halo disturbances, low brightness and low contrast, etc. In this paper, to solve these problems, we propose a foggy image defogging method. First, the nonSubsampled contour transform (NSCT) is employed in this method to partition the image into low and high frequency elements. In order to enhance the preservation of complex information, the Retinex approach utilises a bootstrap filter instead of a Gaussian filter. The denoising method entails the application of a threshold to the high-frequency sub-band pictures. This involves boosting coefficients that surpass the threshold and attenuating coefficients that are below it. The ultimate image is recreated following dehazing by employing the inverse transformation of NSCT. Then, the grey wolf optimization (GWO) algorithm is employed to optimise the regularisation factor of the kernel in the guided filter, hence improving the defogging process. Finally, through extensive experiments, our proposed method outperforms recent approachs under plenty of metrics in terms of visual quality. The method effectively reduces halo aberrations, preserves intricate details, and significantly enhances picture sharpness by reducing atmospheric haze.**

***Index Terms*—nonsubsampled contourlet transform, gray wolf optimization algorithm, image defogging, guided filtering.**

I. Introduction

HAZE is a prevalent meteorological occurrence that is distinguished by the absorption and dispersion of reflected light caused by particles in the atmosphere. The aforementioned issue significantly diminishes the quality of acquired images [1], resulting in undesirable consequences such as object blurring, colour distortion, and decreased contrast [2]. Consequently, these deteriorated images are inadequate for sophisticated visual tasks, such as target identification [3] and self-driving [4], which rely on high resolution images. Haze reduction approaches have attracted substantial attention in the field of image processing and are widely recognised for their enormous practical use.

There are two commonly used defogging algorithms: the physical model and the non-physical model. The physical model approach involves creating an atmospheric scattering model that is based on the principle of picture deterioration. This model is then used to remove fog from images [5]. In the context of image defogging, the conventional air scattering model assumes a uniform distribution of incident light worldwide. However, this model does not accurately represent the actual conditions found in the real world. Yang et al. [6] suggested an improved defogging technique that relies on an atmospheric scattering model. This model demonstrates superior effectiveness compared to traditional air scattering models in terms of recovering visual details in areas with reduced lighting conditions. Wu et al. [7] introduced a technique in their research that tackles the problem of picture defogging by incorporating both the atmospheric scattering model and Retinex. The procedure effectively resolves the problem of reduced contrast and subtle details in images that have undergone defogging recovery operations. The atmospheric scattering models utilise the conventional reduction method to accurately reconstruct the original image by assuming the existence of a black channel before the procedure [8]. In order to tackle the problem of colour distortion and artefacts in the sky region, Wang et al. [9] proposed an adaptive parametric dark channel confidence calculation approach. This correction addresses the difference between the actual transmittance and the expected dark channel a priori region, effectively reducing colour aberrations and artefacts in the reconstructed images. Xie et al. [10] proposed a technique to improve defogging by utilising a dark channel prior and peak signal-to-noise ratio. The proposed methodology seeks to enhance the precision of visual intricacies. Nevertheless, these algorithms, which are grounded in physical models, demonstrate considerable intricacy, hence requiring more stringent criteria.

Another form of defogging technology employs picture enhancing techniques to alleviate the negative impact of fog on image quality. These approaches entail making specific modifications to current picture enhancing algorithms in order to generate improved defogging outcomes. Presently, there exist three primary classifications of defogging algorithms that depend on global-scale image enhancement approaches. One technique used is area segmentation [11], which utilises the optimal orthogonal approximation distribution to divide regions with different distribution characteristics. The template segmentation is customised for different depth modules, and in the end, the block overlapping histogram for the template region is standardised. The approach for picture threshold segmentation, known as the Jensen-Shannon divergence, was introduced by Nie et al. [12]. The segmentation findings have been deemed good. Empirical research indicates that employing this practice is beneficial in improving images with obstructed skies. However, a possible disadvantage of using this specific approach is the occurrence of the block effect. The wavelet transform, as elucidated in the cited reference, is an invaluable technique for mitigating noise in indistinct photos [13]. Sreekala et al. [14] utilised a Gaussian mixture model and wavelet transform methods in

Manuscript received March 1, 2023; revised February 5, 2024.

This work is supported by the National Natural science foundation of China(Grant NO.52174198),and the Construction of Qinchuangyuan Scientists and Engineers Team in Shaanxi Province(2022KXJ-166) the National key research and development program of Shaanxi Province,China(2023 YBSF-133)

Yuanbin Wang is an Associate Professor of Xi'an University of Science and Technology, Shaanxi Xian 710054, China. (Corresponding author,e-mail: wangyb998@163.com)

Bingchao Wu is a postgraduate of Xi'an University of Science and Technology, Shaanxi Xian 710054, China. e-mail: 1598621972@qq.com

Zongyou Duan is a postgraduate of Xi'an University of Science and Technology, Shaanxi Xian 710054, China. e-mail: 1517336423@qq.com

their research, resulting in improved image quality. However, the existing technique lacks a strong sense of orientation and is unable to adequately differentiate between uninterrupted boundaries. Consequently, the photographs that have been defogged have evident flaws in the shape of jagged borders.

Employing advanced directional selectivity is crucial for properly enhancing photos after defogging. The nonsubsampled contourlet transform (NSCT) method [15] is a transformative approach that possesses qualities such as multi-resolution, multi-directionality, translation-invariance, and super-completeness. These properties make it extremely suitable for difficult image processing problems. Employing this particular technology clearly yields advantages in reducing noise and enhancing delicate image features. Moreover, it facilitates the seamless administration of certain regions and objectives for enhancement. However, research suggests that techniques based on NSCT do not significantly improve the visual quality of images with uneven illumination [16].The effectiveness of the third Retinex enhancement algorithm resides in its capacity to efficiently reduce uneven illumination. Nevertheless, it is important to mention that the traditional Retinex technique, which relies on a Gaussian filter, can lead to unwanted artefacts such as 'haloing' and reduced edge sharpness in the image. Wang et al. [17] proposed a technique that combines NSCT (Nonsubsampled Contourlet Transform) with weighted bootstrap filtering to successfully tackle common difficulties in remote sensing imaging, such as low brightness, blurry edges, and limited visibility.The Retinex algorithm employs a weighted filter, as opposed to a Gaussian filter, to obtain intricate and fundamental elements. However, it is challenging to modify the parameter values to match the specific features of the image. Zhang et al. [18] devised a new method with the goal of improving the quality of low-light photos by employing an iterative multi-scale guided filtering Retinex technique. The procedure significantly improves the clarity of image details, but it may result in a disadvantage in the final image, commonly referred to as the 'flooding grey' phenomena. The Retinex approach, with bootstrap filtering, showcases improved preservation of edge details. Nevertheless, the system continues to have difficulties in accurately representing colours, especially as a result of the blurring of sharp differences in brightness when estimating lighted images. Moreover, the magnitude of the regularisation parameter has a substantial impact on the outcomes of the filtering process. The lack of adaptability of the regularisation factor leads to colour distortion during the post-defogging stage of image processing.

This study presents the application of Sigmoid-guided filter-Retinex in the NSCT domain, with the objective of improving the bootstrap filter-Retinex technique. The optimisation of filtering parameters is achieved using the GWO method. At first, when the NSCT is applied to the image, it separates the image into both low-frequency and multiple high-frequency components, each with various orientations. The Sigmoid-guided filter-Retinex technique is used to improve the quality of the low-frequency sub-image. In addition, the GWO method aids in optimising the regularisation factor, resulting in the reduction of halo artefacts and preservation of image features. The high-frequency component subpicture is subjected to a thresholding method to reduce noise and enhance image detail. Afterwards, by employing the NSCT, the image is restored to its initial condition, leading to the production of a clear image. This work conducted extensive testing on a wide range of real-world pictures to compare both subjective visual effects and quantitative indices of this algorithm with three recently proposed image defogging techniques. The results unequivocally validated the exceptional efficacy of the suggested method.

II. ALGORITHM PRINCIPLES

A. NSCT Transform

The Contourlet transform's filter bank structure comprises two main components: the Laplacian pyramid filter (LP) and the directional filter bank (DFB). In order to preserve the band splitting characteristics of the Contourlet transform and attain translation invariance, the NSCT eliminates the process of downsampling from the Contourlet's two-stage transformation and introduces a nondownsampling filter. The structure of this filter is clearly illustrated in Figure 1. The NSCT filter bank demonstrates improved frequency domain selectivity and regularity, resulting in a more efficient subband decomposition. Figure 2(a) demonstrates the utilisation

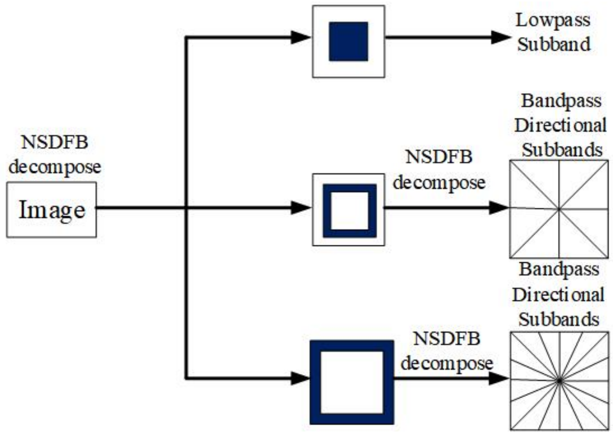

Fig. 1: Nondownsampling Contourlet Filter Bank Structure

of the NSCT transform on the image 'Field', producing one sub-image containing low-frequency components and two sub-images containing high-frequency components. Figure 2(b) exhibits the low-frequency sub-picture, which captures the most fine characteristics visible in the foggy sky image.

B. Retinex Based on Sigmoid and Guided Filtering

This work employs the low-frequency sub-image, which is transformed using NSCT, to recover contour information from the image. Afterwards, the Retinex algorithm is utilised to enhance the overall contrast and visual impact of the image. The guided filter is used because it effectively preserves edges, allowing for accurate estimation and extraction of the illumination component. This process enhances both the contrast and amount of detail in the image effectively. The Retinex hypothesis is a theoretical paradigm that explains the mechanisms involved in how humans perceive brightness and colour. According to the notion, the impression of an object's brightness is affected by both the surrounding ambient illumination and the reflection that comes off the object's surface. In simpler terms, an image can be expressed as the result of combining the light that falls on an object

(a) Forest

(b) Low Frequency Sub-images

Fig. 2: NSCT Transformation of Forest

and the light that bounces off the object. The principle is exemplified by equation (1).

$$I(x,y) = R(x,y) \times L(x,y) \tag{1}$$

I(x,y) is employed to denote the original image. The variable L(x,y) denotes the incident light component of the image. The variable R(x,y) denotes the component of the image that corresponds to the reflected light.

The traditional approach in the Retinex algorithm for estimating illumination involves using a Gaussian filter for computation. However, the Gaussian filter only considers pixel distance in determining filter weights, thus ignoring the actual content of the filtered image. As a consequence, the filtering effect is diminished in its efficacy. In contrast, the guided filter excels in preserving edge details and shows greater efficiency in processing images with large window sizes. Therefore, within the context of the Retinex algorithm for estimating illumination, the guided filter is considered more advantageous than the Gaussian filter.

The guided filtering process involves two maps, the guided map I and the original map P. These maps are filtered and the output is a filter window ω_k. The bootstrap and output maps exhibit local linearity in terms of gradient variation, and are modeled as such. Its principle is shown in equation (2).

$$Q_i = a_k I_i + b_k, \forall i \in \omega_k \tag{2}$$

a_k and b_k are the linear coefficients corresponding to the local window ω_k;i is the pixel index.

When the lead image is the original image there is

$$Q_i = P_i - n_i \tag{3}$$

n_i is noise.

To obtain the coefficients of the linear model, one must transform it into an optimisation problem using an unconstrained image recovery method. The first step is to determine the loss function within the filter window. The principle is exemplified by equation (4).

$$E(a_k, b_k) = \sum_{i \in \omega_k} ((a_k I_k + b_k - P_i)^2 + \epsilon a_k^2) \tag{4}$$

ϵ is the canonical factor to avoid a_k being too large.

Combining equation (2) yields the filtered output image Q as the illumination component L(x,y) of the Retinex algorithm.

(a) Gaussian Filtering

(b) Guided Filtering

Fig. 3: Illumination Components of Gaussian and Bootstrap Filtering

Figure 3 demonstrates that the bootstrap filter outperforms the Gaussian filter in terms of edge detail in the illuminance component. Using directed filtering instead of Gaussian filtering for illuminance estimation in the Retinex algorithm appears to be a feasible alternative.

C. Sigmoid-Guided Filtering-Retinex Algorithm

The histogram of an image taken in foggy weather circumstances usually exhibits a significant level of clustering, mostly as a result of the environmental factors affecting the image. The Sigmoid function exhibits a more prominent spreading impact in comparison to the logarithmic function. The sigmoid function can be mathematically represented by the following equation:

$$sig(x) = \frac{1}{1 + e^{-x}} \tag{5}$$

The Sigmoid function exhibits a flexible change in its point of inflection, which is determined by the alteration of the mean value of the input signal. The Sigmoid function has a greater capacity for adjustment compared to the logarithmic function, indicating a wider range of applicability. Replacing the logarithmic function with the Sigmoid function in the guided filter-Retinex approach yields the following outcome:

$$R(x,y) = sig \frac{I(x,y)}{I(x,y) \otimes F(x,y)} \tag{6}$$

(a) Enhanced Graphs based on Logarithmic Function

(b) Enhanced Graphs based on Sigmoid Function

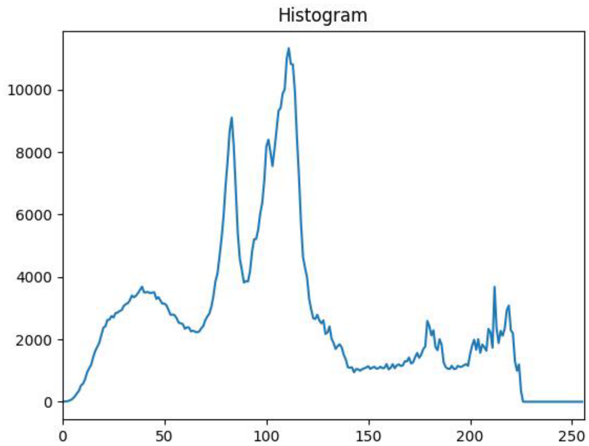

(c) Histograms based on Logarithmic Function

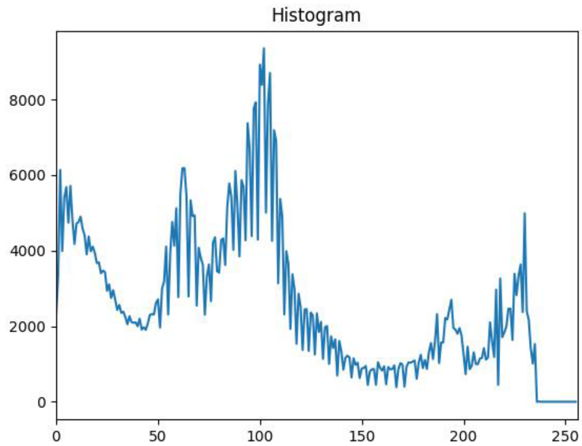

(d) Histograms based on Sigmoid Function

Fig. 4: Logarithmic and Sigmoid Functions Processing Results and Histograms

The image depicted in Figure 2(a) underwent enhancement by the use of logarithmic and Sigmoid function-based guided filter-Retinex algorithms, as demonstrated in Figure 4.

Figure 4(c) and Figure 4(d) indicate that the histogram of the image processed using the Sigmoid function has a wider and more evenly distributed range of grey scale values compared to the histogram of the image processed with the logarithmic function.

D. Threshold Denoising

Upon using NSCT on the image, it becomes evident that specific regions of the image, which depict high-frequency information, unveil the intricate and subtle elements of it. Smaller absolute values of coefficients generally suggest a greater presence of noise components. Conversely, coefficients with greater magnitudes are typically associated with reduced levels of noise and an augmentation in the amount of information. Thus, it is possible to set a threshold, referred to as T expressly for excluding high-frequency sub-band coefficients. This thresholding technique significantly reduces noise while preserving important information in the image. In order to clarify, coefficients that are lower than a preset threshold are adjusted to zero, effectively reducing or eliminating unwanted disturbances. Threshold shrinkage is a widely used approach in image processing, which involves two main methods: hard threshold shrinkage and soft threshold shrinkage. Every approach possesses unique operational features and specific applications in the field of noise reduction. The utilisation of hard threshold shrinking has proven to be effective in addressing the persistent deviation found while using soft thresholding. This is particularly significant in situations where there are high-frequency coefficients that surpass a set threshold. The use of this technique is essential for decreasing distortions, such as blurring at the edges, and has the potential to enhance the image's peak signal-to-noise ratio, so emphasising the characteristics of edge details. Therefore, in our investigation, we have opted to utilise a hard threshold shrinkage function. This function aims to reduce the high-frequency sub-band coefficients in order to attenuate noise. The adjustment of the coefficients is performed using equation (7).

$$C_k^{j'} = \begin{cases} C_k^j & |C_k^j| > T \\ 0 & otherwise \end{cases} \quad (7)$$

C_k^j with $C_k^{j'}$ are the coefficient of high frequency before and after processing and T is the threshold value.

If a uniform threshold is applied to analyse each subband, it may not yield a precise estimation of the noise and edge regions inside each subband. The determination of the threshold is contingent upon the subband coefficients with high frequency, resulting in the selection of distinct thresholds for varying scales and directions. Additionally, the threshold is set proportionally to the standard deviation of the transform coefficients [19], i.e.

$$T = \frac{1}{2}\sqrt{\frac{1}{M \times N}\sum_{x=1}^{M}\sum_{y=1}^{N}(C_k^j(x,y) - mean_c)^2\sigma} \quad (8)$$

$C_k^j(x,y)$ is the coefficient of the kth subband at (x,y) at the jth scale, $mean_c$ is the mean value of the coefficients within that subband. M and N are the dimensions of the image, σ is calculated from the empirical formula for wavelet noise estimation shown in equation (9) obtains.

$$\sigma^2 = Median[h_k^j/0.6745] \quad (9)$$

The process of applying threshold denoising to the high-frequency sub-band pictures was executed, and the outcomes are visually presented in Figure 5. This method introduces

(a) First HF Sub-image Threshold Denoising

(b) Second HF Sub-image Threshold Denoising

Fig. 5: High Frequency Processing Results

a novel strategy for estimating the threshold value, building upon the conventional hard thresholding shrinkage technique. Instead of employing a static thresholding technique, the proposed method operates under the assumption that the transformation coefficient exhibits proportionality with the threshold value. The method attains a balance in denoising various regions by choosing the threshold value according to the transformation coefficient. Figure 5 illustrates the efficacy of the proposed methodology in enhancing the level of detail in foggy sky images while simultaneously reducing noise.

E. Grey Wolf Algorithm Optimization Process

The regularisation parameter of the bootstrap filter kernel has a considerable impact on the results of the defogging process. By reducing the regularisation factor, the elimination of the reflecting component of the halo can be enhanced. Nevertheless, this results in a decrease in the range of grey values. On the other hand, increasing the regularisation factor intensifies the halo phenomena, while simultaneously expanding the dynamic range of the grey values.

Figure 6 demonstrates that a reduced regularisation factor successfully reduces the occurrence of halo phenomena. On the other hand, increasing the regularisation factor worsens the halo effect, hence reducing the visual quality of the image. In order to further evaluate the filtering impact, one

(a) Original Image

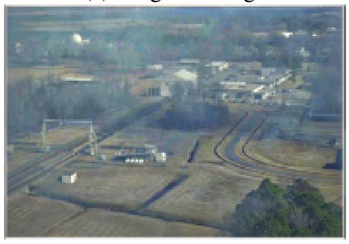

(b) ϵ =0.05

(c) ϵ =0.08

(d) ϵ =0.1

Fig. 6: Filtering Results for Different Values of ϵ

can modify the parameter value and review the resulting smoothed image using the average gradient as the criterion for evaluation. This assessment is based on the possibility for improving the picture quality through bootstrap filtering. The equation (10) represents the mathematical formula employed for calculating the mean gradient.

$$AG = \frac{1}{M \times N}\sum_{x=1}^{M}\sum_{y=1}^{N}\sqrt{\frac{(\frac{\partial f(x,y)}{\partial x})^2 + (\frac{\partial f(x,y)}{\partial x})^2}{2}} \quad (10)$$

$M \times N$ indicates the size of the image, $\frac{\partial f}{\partial x}$, $\frac{\partial f}{\partial y}$ indicating the horizontal and vertical gradients respectively.

Figure 6(a) was chosen to calculate the average gradient AG after smoothing with different regularisation factors ϵ, as shown in Figure 7.

Figure 7 demonstrates that the level of smoothing escalates logarithmically as it becomes more pronounced. However, it is important to recognise that this process does have its

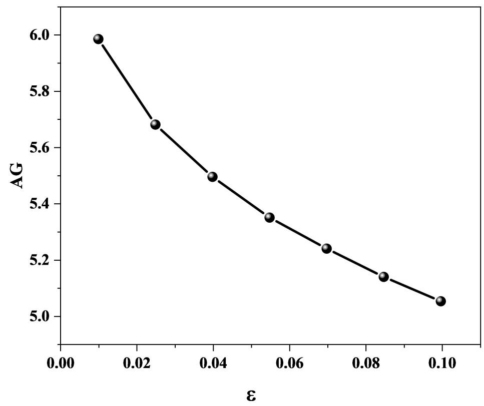

Fig. 7: Trends in AG at Different ϵ

drawbacks, including the occurrence of halos and colour distortion.

To enhance the efficiency of defogging by the modification of the regularisation factor, it is essential to develop an appropriate fitness function that enables quantitative assessment.This study employs the multiplication of contrast and information entropy as the fitness function to evaluate the quality of the defogged image, taking into account both the contrast and information entropy assessment indices. The choice of the grey wolf algorithm as the regularisation factor is based on its ability to overcome local optima during parameter optimisation and its efficient execution time. Equations (11) and (12) illustrate the calculation of contrast and entropy.

$$Constract = \frac{1}{M*N}\sum_{m}^{i=1}\sum_{n}^{j=1}E^2(i,j)-|\frac{1}{M*N}\sum_{m}^{i=1}\sum_{n}^{j=1}E(x,y)|^2 \tag{11}$$

$$Entropy = -\sum_{L-1}^{i=0}D(i)log_2D(i) \tag{12}$$

$$Fitness = Constract \times Entropy \tag{13}$$

M and N are the width and height of the image respectively, (i,j) denoting the pixel positions, and E(i,j) are the pixel grey scale values. D(i)is the ratio of the number of pixels N(i) with a grey scale value of i to the total number of pixels N in the image, i.e. $P(i) = N(i)/N$.

The fitness function, denoted as equation (13), is defined as the multiplication of contrast and entropy.

The fundamental principle of the GWO algorithm [20] involves simulating the hierarchical leadership structures and collective hunting activities observed in packs of grey wolves. Grey wolf packs in their native habitat exhibit a strict social hierarchy, in which all pack members are classified into four distinct classes. The alpha designation is bestowed upon the individual with the utmost fitness value, whilst the beta and gamma designations are bestowed upon individuals with the second and third greatest fitness values respectively. The remaining persons are classified as delta. The grey wolves from each class work together closely to efficiently locate the most appropriate prey source through repeated cyclical processes, aiming to establish the best search criteria, as described in the stated research article. The main goal of this algorithm is to gain a deeper understanding of the dynamics of grey wolf populations in relation to their prey.

$$D = |C \cdot X_p(t) - X(t)| \tag{14}$$

$$X(t+1) = X_p(t) - A \cdot D \tag{15}$$

$X(t)$ and $X(t+1)$ denote the position of the grey wolf at the (t)th and $(t+1)$th iteration, respectively, $X_p(t)$ denote the position of the prey at the (t)th iteration, is the distance between the individual grey wolf and the prey, A and C are coefficient vectors, calculated from equations (16) and (17).

$$A = 2\alpha r_1 - \alpha \tag{16}$$

$$C = 2r_2 \tag{17}$$

r_1 with r_2 are [0,1] random vector; α is a convergence factor that decreases linearly from 2 to 0.

In wolf packs, other grey wolves usually use the position of the wolf to locate prey and keep updated on.

$$\begin{cases} D_\alpha = |C_1 \cdot X_\alpha - X| & X_1 = X_\alpha - A_1 \cdot D_\alpha \\ D_\beta = |C_2 \cdot X_\beta - X| & X_2 = X_\beta - A_2 \cdot D_\beta \\ D_\delta = |C_3 \cdot X_\delta - X| & X_3 = X_\delta - A_3 \cdot D_\delta \end{cases} \tag{18}$$

$$X(t+1) = \frac{X_1 + X_2 + X_3}{3} \tag{19}$$

III. ALGORITHM FLOW IN THIS PAPER

The grey wolf method is employed in conjunction with the NSCT domain improvement algorithm to effectively explore the best value of the regularisation factor and ultimately complete the process of image defogging. The steps of the algorithm are as follows.

(1) To study the image, it is imperative to break it down into sub-images with high-frequency and low-frequency components using NSCT (Non-Subsampled Contourlet Transform). After decomposing the image, the sub-images with high frequencies undergo denoising using equations (7) and (8).

(2) The starting population is defined as N = 50, the maximum number of iterations is defined as 100, and the search dimension is defined as 2. Furthermore, the range of the regularisation factor for the kernel of the bootstrap filter is set to [0.01, 1].

(3) Initialize the population orientation of the wolves, i.e. ϵ .The initial value of the Sigmoid-guided filtering-Retinex enhancement of the low-frequency part of the image using this parameter.

(4) The adaptation value is calculated according to equation (13) to evaluate the defogging effect, α β δ wolves are selected based on the fitness value, their positions are the optimal, superior and sub-optimal solutions. The wolves evaluate the current position of the prey and the remaining wolves evaluate their own position and follow.

(5) To update the position of the grey wolf population, equation (15) is utilised.

(6) Once the wolf scouted the location of the prey during hunting in the grey wolf population, they directed the wolves to approach the prey until it was captured, according to the α ,A,C value updated in equations (16) and (17).

(7) After completing 100 iterations, the best answer at a global level is identified as the most advantageous value for the enhancement parameters examined in this research study. The Sigmoid-guided filter-Retinex outputs the ideal parameter values to enhance the image of a foggy sky and reduce the foggy effect. The resultant outcome is subsequently combined with the high-frequency sub-image that underwent processing in step (1), and then subjected to an inverse transformation to produce the dehazed image.

IV. EXPERIMENTAL RESULTS AND ANALYSIS

The experimental and simulation results were computed using a personal computer. The simulation environment utilised was Matlab 2019a. The computer's CPU was an Intel i5-12490F, with a memory capacity of 16 GB. The operating system employed was Windows 10.

To assess the efficacy of the algorithm proposed in this research paper for enhancing defogging, a comparative analysis is conducted with the single-scale Retinex (SSR), multi-scale Retinex (MSR), and guided filtering algorithms. The algorithm in question is evaluated from both subjective and objective perspectives.

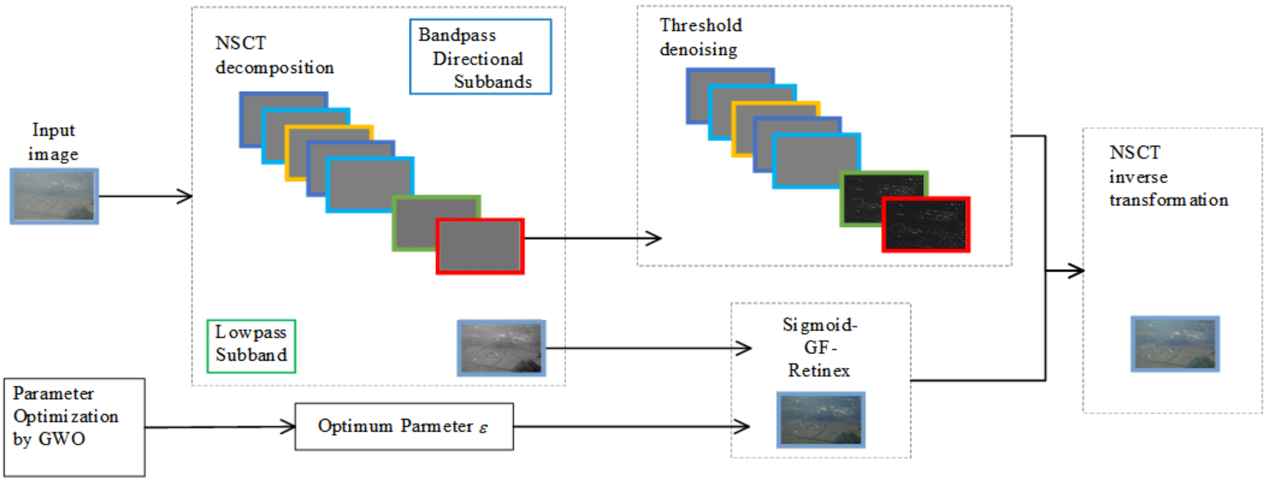

Fig. 8: Framework Diagram for This Article

Fig. 9: Defogging Images Obtained by Different Algorithms

A. Subjective Aspects

Figure 9 analysis demonstrates that the SSR algorithm enhances image features to a considerable extent. Nevertheless, this improvement is accompanied by significant colour distortion and a minor halo effect. Conversely, the MSR algorithm demonstrates a superior benefit in terms of colour preservation when compared to the SSR algorithm. However, it continues to experience issues with colour distortion and the halo effect. Moreover, the incapacity to handle various images in separate ways exacerbates colour distortion, leading to bad visual outcomes for cloudy images. This study showcases the algorithm's capacity to augment image edge detail information and boost image contrast. Nevertheless, it fails to demonstrate substantial enhancements in image luminosity. Moreover, the algorithm possesses the capability to improve the visual clarity of the image and effectively reduce the halo effect that frequently arises following the application of the conventional Retinex algorithm for fog elimination. This achievement is credited to the optimisation of the guide filter parameters.

B. Objective Aspect

The grey wolf algorithm optimizes the bootstrap filter parameters ϵ for each of the six images, and the iterative diagram of the optimisation process is shown in Figure 10.

As can be seen from Figure 10, the functions all reach convergence when the number of iteration is 20. In this paper, the guided filter parameter of the unoptimized algorithm is taken as ϵ=0.01, and the final parameter values after the grey wolf algorithm seeking optimization are shown in Table 1.

As seen in Table 1, the grey wolf algorithm determines the optimal bootstrap filtering parameters for each image, resulting in the highest quality image outcomes. As depicted in Table 1, the

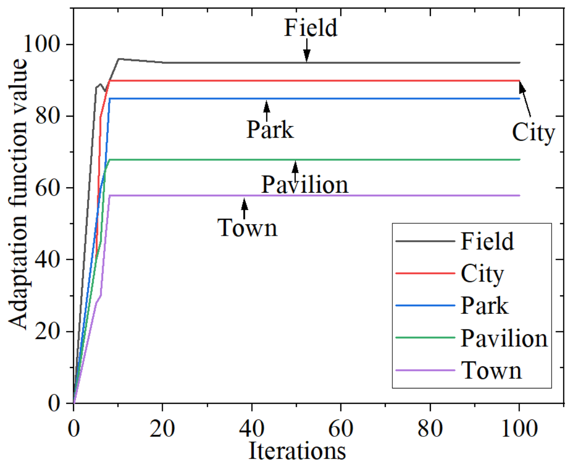

Fig. 10: Iteration Diagram of the Grey Wolf Algorithm for Finding the Best Process

TABLE I: PARAMETER VALUES BEFORE AND AFTER BOOTSTRAP FILTERING OPTIMIZATION

Parameter	Not optimised	Value of search results					
		Field	City	Park	Pavilion	Town	Sky
ϵ	0.01	0.04	0.04	0.05	0.04	0.01	0.08

grey wolf algorithm effectively determines the optimal bootstrap filtering settings for individual images, resulting in superior image outcomes.

When assessing the quality of an image, objective indicators tend to be more persuasive. To ascertain the credibility of an image, it is often more persuasive to rely on objective signs during the evaluation process. To ascertain the efficacy of the method proposed in this paper for addressing the issues of halo artefacts and inconspicuous details inherent in the conventional Retinex defogging algorithm, the authors have incorporated the parameter of Spatial Frequency (SF) in addition to employing contrast and information entropy, as defined in equations (13) and (14), as evaluation metrics for the algorithm. The inclusion of SF enables an effective assessment of image clarity. As the spatial frequency increases, the image becomes more distinct.

$$RF = \sqrt{\frac{1}{mn}\sum_{i=1}^{M-1}\sum_{j=1}^{N-1}(F(i,i)-F(i,j+1))^2} \tag{20}$$

$$CF = \sqrt{\frac{1}{mn}\sum_{i=1}^{M-1}\sum_{j=1}^{N-1}(F(i,i)-F(i+1,j))^2} \tag{21}$$

$$SF = \sqrt{RF^2 + CF^2} \tag{22}$$

RF and CF indicate the row frequency and column frequency of the image respectively. The results displayed in Table 2 demonstrate that the image, which was subjected to the algorithm suggested in this research, demonstrates higher performance in terms of contrast, information entropy, and spatial frequency in comparison to both the SSR algorithm and MSR method. Nevertheless, it is important to acknowledge that the subjective assessment of Figure 9 indicates that the image, which underwent processing by the SSR method, has evident colour distortion. Moreover, the algorithm presented in this work exhibits superior performance in terms of information entropy data when compared to guided filtering. This indicates that the suggested technique produces more complex results after removing fog from the image. Moreover, the methodology described in this academic paper effectively reduces the halo effect and colour aberration commonly observed in traditional Retinex algorithms when processing photographs influenced by air haze. Furthermore, it displays an improved ability to retain specific information. Furthermore, the approach outlined in this research study showcases improved visual outcomes in terms of excessive augmentation when compared to the conventional Retinex algorithm.

In order to further verify the generalization of the model and the superiority of the proposed algorithm, this paper introduces the peak signal-to-noise ratio(PSNR) and structural similarity(SSIM) as objective indexes for measuring the algorithm's defogging performance. The principles are shown in equation (23) and (24). In the equation, MSE is the mean square error of the two images, n is 255; μ_x and μ_y are the average of all pixels in the image, δ_x and δ_y are the standard deviations of all image pixels. A higher PSNR value indicates better image reconstruction quality, although it may not accurately represent the subjective perception of human eyes; A higher SSIM value corresponds to a smaller difference between the two pictures, indicating a more effective fog removal effect. The experimental results of the proposed algorithm and the comparison algorithm on the O-HAZE [21] dataset are shown in Table 3.

$$PSNR = 10 \times lg|\frac{(2^n-1)^2}{MSE}| \tag{23}$$

$$SSIM = \frac{2\mu_x\mu_y + C_1}{\mu_x^2 + \mu_y^2 + C_1} \times \frac{2\delta_{xy} + C_2}{\delta_x^2 + \delta_y^2 + C_2} \tag{24}$$

Table 3 displays the mean metrics of the algorithm employed in this study and the comparative algorithm on the O-HAZE dataset. The results suggest that the algorithm employed in this study surpasses the comparative algorithm in terms of assessment metrics, including Entropy, SF, PSNR, and SSIM. Indications are that the algorithm put forth in this study has the potential to effectively enhance image quality and possesses superior dehazing capabilities compared to the dehazing algorithms commonly employed in mainstream research.

V. CONCLUSION

This paper presents a new method for enhancing the Retinex defogging algorithm by optimising it in the NSCT domain. The suggested approach integrates the GWO algorithm with a Sigmoid-guided filtering methodology to effectively address the difficulties given by halo artefacts and inconspicuous details. The proposed

TABLE II: OBJECTIVE EVALUATION RESULTS OF IMAGE QUALITY OBTAINED BY DIFFERENT ALGORITHMS

Test images	Evaluation indicators	SSR	MSR	Guided Filtering	Proposed
	Contrast	78.1737	317.9633	**401.2678**	335.5292
Field	Entropy	2.3903	3.2981	2.2766	**3.5414**
	SF	6.7847	18.0188	13.9495	**18.7784**
	Contrast	162.1129	345.8684	**399.0024**	367.2635
City	Entropy	3.8458	4.5284	2.3467	**4.9037**
	SF	20.4672	22.9323	16.4799	**23.6436**
	Contrast	101.0305	279.3230	**316.0348**	288.3645
Park	Entropy	4.2713	4.3895	2.3714	**4.4815**
	SF	18.3124	19.3259	16.1513	**21.8546**
	Contrast	88.0305	298.6611	**340.7963**	314.3645
Pavilion	Entropy	3.8458	4.2332	2.3084	**5.1231**
	SF	8.3694	19.8079	16.5714	**20.1259**
	Contrast	108.9536	250.9001	**275.5428**	260.9148
Town	Entropy	2.6789	4.9141	2.3147	**4.9580**
	SF	15.5047	19.1020	19.0416	**20.0612**
	Contrast	94.3469	228.1476	**230.6086**	150.1077
Sky	Entropy	2.5986	3.1295	2.9068	**3.1479**
	SF	8.9103	13.5108	12.2813	**13.7936**

TABLE III: THE EXPERTIMENTAL RESULTS OF EACH MODEL IN O-HAZE DATASET

Parameter \ Model	SSR	MSR	Proposed
Contrast	105.21	286.10	**286.93**
Entropy	3.27	4.08	**4.36**
SF	13.05	18.78	**19.71**
PSNR	15.24	17.11	**22.06**
SSIM	0.82	0.67	**0.86**

approach offers significant advantages in enhancing both image contrast and information entropy. In addition, the grey wolf algorithm is used to automatically determine the optimal regularisation factor in the guided filtering process, hence enhancing the program's inherent adaptability. This feature enables the system to automatically find the optimal boosting parameters for different images taken in foggy situations, resulting in the most efficient defogging result. The experimental results indicate that the defogging image generated by this study successfully reduces halo artefacts while maintaining the fine characteristics of the image. Furthermore, the defogging effect exceeds that of often employed defogging algorithms, thereby greatly improving the image quality. The results demonstrate that the technique suggested in this research is highly feasible and has significant relevance for practical applications.

REFERENCES

[1] H. Hu, Q. Guo,J. Zheng et al., "Single Image Defogging Based on Illumination Decomposition for Visual Maritime Surveillance", *IEEE Transactions on Image Processing*, vol. 28, no. 6, pp. 2882-2897, 2019.

[2] X. Min, G. Zhai, K. Gu et al., "Quality evaluation of image dehazing methods using synthetic hazy images", *IEEE Transactions on Multimedia*, vol. 21, no. 9, pp. 2319-2333, 2019.

[3] J. Cao, P. H. Li, H. Zhang et al., "An Improved YOLOv4 Lightweight Traffic Sign Detection Algorithm", *IAENG International Journal of Computer Science*, vol. 50, no. 3, pp. 825-831, 2023.

[4] G. H. Tian, P. J. Dai, "Active collision avoidance method of driverless vehicle based on partheno genetic algorithm", *Journal of Jilin University (Engineering Edition)*, vol. 53, no. 8, pp. 2404-2409, 2023.

[5] M. Y. Ju, C. Ding ,W. Q. Ren et al., "Image Dehazing and Exposure Using an Enhanced Atmospheric Scattering Model", *IEEE Transactions on image processing*, vol. 30, no. 18, pp. 2180-2192, 2021.

[6] Y. Yang, G. Qiu, S. Huang et al., "Single image dehazing method based on improved atmospheric scattering model", *Journal of Beijing University of Aeronautics and Astronautics*, vol. 13, no. 8, pp. 1364-1375, 2022.

[7] X. Wu, Q. Gao, S. Huang et al., "Adaptive Retinex Image Defogging Algorithm Based on Depth-of-Field Information", *Laser & Optoelectronics Progress*, vol 60, no. 12, pp. 160-169, 2023.

[8] X. Zhang, K. Xing, Q. F. Liu et al., "Single Image Reflection Removal Based on Dark Channel Sparsity Prior", *IEEE Transactions on Circuits and Systems for Video Technology*, vol. 33, no. 11, pp. 6431-6442, 2023.

[9] S. Wang, J. Chen, "Dark Channel Prior Defogging Algorithm for Adaptive Correction Transmittance", *Computer Engineering and Applications*, vol. 57, no. 13, pp. 207-211, 2021.

[10] L. Xie, G. Xiong, B. Yu et al., "A new method for atmospheric degradation image defogging based on dark channel a priori", *Control Engineering*, vol. 27, no. 2, pp. 207-211, 2020.

[11] A. W. Rosyadi, N. Suciati, "Image segmentation using transition region and k-means clustering", *IAENG International Journal of Computer Science*, vol. 47, no. 1, pp. 47-55, 2020.

[12] F. Y. Nie, J. Q. Li, "Image Threshold Segmentation with Jensen-Shannon Divergence and Its Application", *IAENG International Journal of Computer Science*, vol. 49, no. 1, pp. 200-206, 2022.

[13] P. Zhen, B. Zhang, Z. Chen et al., "Spectrum sensing method based on wavelet transform and residual network", *IEEE Wireless Communications Letters*, vol. 11, no. 12, pp. 2517-2521, 2022.

[14] K. Sreekala, H.C. Sateesh Kumar, K. B. Raja, "Denoising of Low Light Images using Patch Priors and Wavelets", *Engineering Letters*, vol. 29, no. 3, pp. 1248-1263, 2021.

[15] C. Li, X. Wen, X. Liu et al., "Simultaneous seismic data interpolation and denoising based on nonsubsampled contourlet transform integrating with two-step iterative log thresholding algorithm", *IEEE Transactions on Geoscience and Remote Sensing*, vol. 60, pp. 1-10, 2022.

[16] Y. WU, J. Shi, "Non-subsampled Contourlet domain image enhancement based on multiscale Retinex", *Journal of Optics*, vol. 35, no. 3, pp. 87-96, 2015.

[17] S. Wang, X. Zhou, "Remote sensing image enhancement based on non-downsampled contour wave transform and weighted bootstrap filtering", *Advances in Laser and Optoelectronics*, vol. 57, no. 12, pp. 230-236, 2020.

[18] J. Zhang, P. Zhou, Q. Zhang, "Low-illumination image enhancement based on iterative multiscale guided filtering Retinex", *Journal of Graphology*, vol. 39, no. 1, pp. 1-11, 2018.

[19] M. Wang, Z. Tian, "Mine image enhancement algorithm based on non-downsampling contour wave transform", *Journal of Coal*, vol. 45, no. 9, pp. 3351-3362, 2020.

[20] W. Long, T.Wu, M.Tang et al., "Grey wolf optimization algorithm

based on lenticular imaging learning strategy", *Journal of Automation*, vol. 46, no. 10, pp. 2148-2164, 2020.

[21] Y.Li, Y.Liu, Q. X. Yan et al., "Deep Dehazing Network With Latent Ensembling Architecture and Adversarial Learning", *IEEE Transactions on Image Processing*, vol. 30, pp. 1354-1368, 2021.